Chapter 2

Frequency and time-domain analyses of multiple reflections and interference phenomena in a metamaterial absorber

2.1. Introduction

During the last few years, a growing interest has been exhibited by the researchers in the study of metamaterial based absorber of electromagnetic radiation due to their compact size and high absorption capacity [38-47]. A metamaterial absorber involves a metal-dielectric-metal, tri-layer structure wherein the top layer is a metasurface consisting of sub-wavelength sized periodically arranged metallic structures; the middle layer comprises a dielectric material while the bottom layer is a metallic reflector. The constitutive electromagnetic properties of the structure can be tailored artificially by adjusting the dimensions of the periodically arranged metallic structures and the thickness of the dielectric material. The theory of absorption of electromagnetic radiation by a metamaterial was initially evolved based on a single-layer effective model where the whole metamaterial structure was considered as a single atom having effective constitutive electromagnetic parameters. These constitutive parameters are highly dispersive and thereby can be tailored easily. By properly tuning the geometrical dimensions of the periodically arranged metallic structures, the effective impedance of the absorber can be made equal to the intrinsic impedance of the free space; thereby, providing an impedance matching condition for the incident electromagnetic wave. Therefore, the electromagnetic wave impinging on the top surface of the metamaterial absorber enters into the structure

without any reflection [48]. The presence of metallic reflector at the bottom prevents any transmission from the structure. In this way, the electromagnetic wave entering inside the middle layer gets trapped and perfectly absorbed in the structure subjected to the condition that the simultaneous excitation of electric and magnetic resonances at the resonating frequency is ensured. The metal at the top layer is responsible for the electric resonance, whereas the occurrence of antiparallel surface currents between the top and the bottom metallic plates is responsible for the magnetic one [49]. These absorbers are useful in thermal detection [50], bolometer [51], enhancing solar cells efficiency [52], plasmonic sensors [53], and infrared photo detectors [54].

Earlier, a few works have been done on proposing a new theory of absorption based on multiple interference model. The work done in [55] has discussed the formation of Fabry-Perot resonance in a quarter wavelength size dielectric. The dependency of dielectric cavity thickness on wavelength restricts this method to be used for narrow band metamaterial absorbers only. Also, the quarter wavelength size makes the structure bulky in nature. Similarly, the work presented in [56-57], has explained metamaterial absorber based on multiple interference method. But, from these works, it is not clear that whether multiple interference theory is an alternative theory for metamaterial absorption (other than single model theory, based on electric and magnetic resonances) or whether it is the only theory to explain metamaterial absorption. In other words, it couldn't explain the validity of absorption based on single model theory.

The theory of metamaterial absorption based on single atom theory becomes questionable when the electromagnetic radiation is incident from the bottom side, instead from the top side. If a metasurface absorber is incident from the bottom side, then a complete reflection takes place, despite the fact that effective impedance of the metamaterial structure is equal to the intrinsic impedance of free space. This asymmetric nature of the metamaterial structure cannot be

explained by modelling the metamaterial structure as a single atom/entity. Further, we found that with each integral increment of a half-wavelength in the dielectric thickness, the absorption characteristics repeat itself. An ambiguity between absorption characteristics and surface current components was found when the increment was for an odd integral value of a half-wavelength. For this case, the absorption characteristics repeat itself, despite the fact that the surface current remains parallel to each other. This contradicts the single effective medium theory for which the occurrence of anti-parallel surface current is believed to be responsible for perfect absorption. To explain the metamaterial absorption characteristics multiple reflection interference model has been considered in this chapter. The absorption characteristics is explained on the basis of three-layer model which treats metamaterial structure as an assembly of three different functional layers. The reflection and absorption characteristics of the whole structure can be obtained by multiplying the reflection and absorption coefficient of each layer. The reason for absorption at higher-order cavity along with the reason for parallel and antiparallel surface currents can be well explained implementing this model. Furthermore, for the first time, a time-domain analysis of metamaterial absorber under normal incidence as well as oblique incidence has been carried out to validate the existence of multiple reflection phenomenon existing inside the structure. This is done by converting the frequency-domain reflection coefficient of the structure into the time-domain one using inverse chirp-Z transform technique.

2.2. Theoretical analysis of absorption based on three-layer model

For the frequency and time domain analysis of multiple reflection interference model, a typical narrowband metamaterial absorber operating at 10 μm wavelength has been considered. All the simulation has been done in CST Microwave studio employing periodic boundary conditions. The top and the side views of the unit cell of the absorber along with the electric field, magnetic field, and wave vector directions are shown in Fig. 2.1(a) and Fig. 2.1(b),

respectively. The structure (Fig. 2.1(b)) consists of three layers e.g., a resonating metasurface on the top, a dielectric layer at the middle and a metallic reflector at the bottom. For all the metallic components, gold has been chosen owing to its good chemical stability, low ohmic losses, and ease in nano-fabrication. The dielectric permittivity of gold has been modelled using Drude expression given in equation (2.1)

$$\varepsilon(\omega) = 1 - \frac{\omega_p^{\,2}}{\omega(\omega + i\gamma)} \tag{2.1}$$

The plasma frequency and damping frequency are 2176 THz and 5.9 THz respectively [58]. ZnSe has been chosen as dielectric due to its good thermal and mechanical properties at THz/Infrared frequencies. The dielectric permittivity of ZnSe in the desired frequency range has been taken from the data available in [59]. The thickness of the dielectric is taken as 0.28 µm. The simulated absorptivity response for the optimized dimensions of the structure is shown in Fig. 2.1(c). It is observed from Fig. 2.1(c), that the structure shows a maximum absorptivity of more than 95% at 10 µm. For absorption at 10 µm, the geometrical dimensions of the unit cell shown in Fig. 2.1(a) are optimized as a = 1.7 µm, b = 1.4 µm, c = 0.1 µm, d = 0.1 µm, e = 0.2 µm.

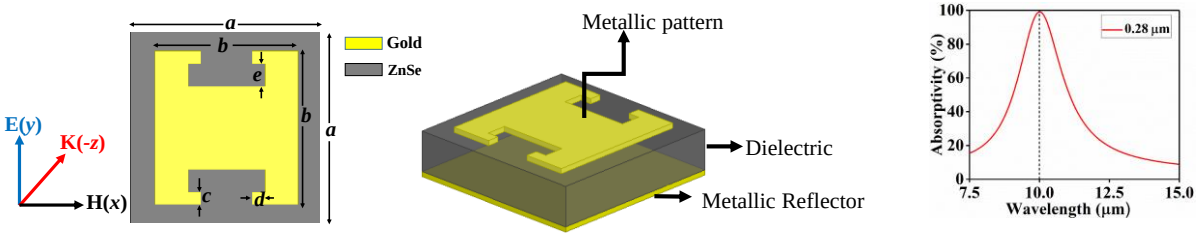

Fig. 2.1. Schematic of the (a) top view; (b) side view of the proposed unit cell along with the incident electromagnetic field directions and (c) absorptivity response of the structure.

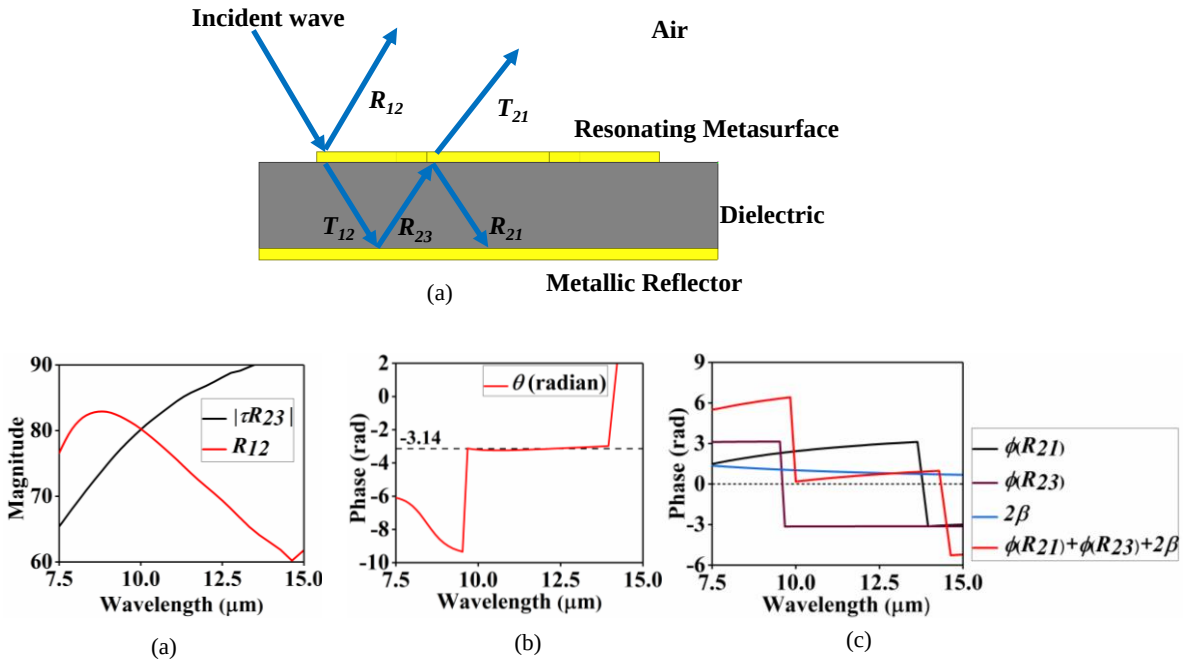

Fig. 2.2 (a) Multiple reflections and transmissions coefficients at each layer of the metamaterial absorber (b) amplitude and (c) phase condition for zero reflection at 10 μm (d) phase condition confirming FP resonance formation inside the dielectric cavity for the structure whose unit cell is shown in Fig. 2.1.

2.3.. Multiple reflections phenomenon inside the dielectric layer

To understand the absorption mechanism, a schematic diagram showing multiple reflections and transmissions of waves at each layer of metamaterial absorber is illustrated in Fig. 2.2(a). When the electromagnetic wave is incident on the top metasurface, a part of the wave undergoes reflection whereas the rest of the wave enters into the cavity (dielectric layer) and undergoes multiple reflections between the top and bottom metallic plates. The overall reflection of the metamaterial absorber structure whose unit cell is shown in Fig. 2.1(a) is obtained by multiplying the transmission and reflection coefficient of each layer [60]. The net reflection of the structure is given by equation (2.2), where R_{12} and R_{21} are the reflection coefficients of the top resonating metasurface from the front (i.e. air) side and the back (i.e. dielectric) side respectively, the reflection coefficient of the metallic reflector is shown as R_{23} .

$$r_{structure} = \frac{R_{12} + \tau R_{23} e^{2i\beta}}{1 - R_{21} R_{23} e^{2i\beta}} \tag{2.2}$$

Here, τ is equal to $T_{21}T_{12} - R_{12}R_{21}$, where T_{12} and T_{21} are the transmission coefficients of the resonating metasurface from the front (i.e. air) side and back (i.e. dielectric) side respectively. $\beta = \eta \times k \times t_d$ is the phase change experienced by the wave as it travels inside the cavity, η is the refractive index of the medium, k is the propagation vector and t_d is the dielectric thickness. To simulate the reflection and transmission coefficients, the whole metamaterial absorber has been decoupled into two tuned surfaces i.e., air-metasurface-dielectric and dielectric-metallic reflector configurations. The reflection and transmission coefficients linked with the top metasurface layer R_{12}, R_{21}, T_{12} and T_{21} can be obtained by simulating air-metasurface-dielectric configuration, whereas the reflection coefficient R_{23} can be obtained by simulating dielectric-metallic reflector configuration [61]. From equation (2.2), the amplitude and phase conditions for $r_{strcuture} = 0$ are derived and are given by equations. (2.3) and (2.4) respectively.

$$R_{12} = \left| \tau R_{23} \right| \tag{2.3}$$

$$\theta = \phi(R_{12}) - \phi(R_{23}) - \phi(\tau) - 2\beta = (2n+1)\pi, \ |n| = 0, 1, 2\ldots$$

(2.4)

θ is the total phase difference between the phase of the reflection and transmission coefficients given in the numerator of equation (2.2). $\phi(R_{12})$ is the phase of the coefficient R_{12}, $\phi(\tau)$ is the total phase associated with the constant τ, $\phi(R_{23})$ is the phase associated with the reflection coefficient R_{23}, whereas 2β is the total phase change experienced by the wave as it propagates inside the cavity. Both the amplitude and phase conditions are evaluated for the structure whose unit cell is shown in Fig. 2.1(a). It can be seen from Fig. 2.2(b) and Fig. 2.2(c) that both the amplitude and phase conditions for zero net reflection are simultaneously satisfied at 10 μm only. This signifies that at resonating wavelength all the wave incident on the top metasurface

enters into the dielectric cavity without any reflection. The wave after entering the dielectric cavity gets reflected multiple times between the two parallel metallic plates. This structure consisting of two parallel metallic plates separated by a dielectric resembles a typical Fabry-Perot cavity. The Fabry-Perot cavity resonance can be established when the total phase change experienced by the wave in a round trip is equal to $2n\pi$ as by equation (2.5); *n* being the integer.

$$\varphi = \phi(R_{21}) + \phi(R_{23}) + 2\beta = 2n\pi, \ |n| = 0,1,2.. \tag{2.5}$$

In this way, the multiple reflected waves inside the cavity are in phase and thus interfere constructively leading to Fabry-Perot resonance modes, resulting in absorption peaks [60]. It can be easily seen from the curve shown in Fig. 2.2(d) that at the wavelength of interest (i.e., 10 μm), the value of φ comes out to be zero; thus, satisfying the necessary condition for the resonance.

By proper analyses of the phase conditions mentioned in equations (2.4) and (2.5), it is evident that the phase condition remains invariant if there is an increment of $2n\pi$ in β. An increment of $2n\pi$ in β corresponds to an increment of $n\frac{\lambda_d}{2}$ in the cavity thickness, where λ_d corresponds to the wavelength inside the cavity and n is the integer. An increment in *n* decides the order of the cavity and is also responsible for higher-order Fabry-Perot resonance modes. In order to verify the effect of higher order cavity thickness on absorptivity, the absorptivity response of the structure whose unit cell is shown in Fig. 2.1(a) has been studied for the first three orders of cavity thickness. The absorptivity responses for the first three orders of cavity thickness, e.g., 1st ($t_{d1} = 0.28$ μm), 2nd ($t_{d2} = 0.28 + \frac{\lambda_d}{2} = 2.38$ μm) and 3rd ($t_{d3} = 0.28 + \lambda_d = 4.48$ μm) have been shown in Figs. 2.3(a)-(c) respectively. It has been observed that the absorption characteristics repeat itself at 10 μm irrespective of the order of cavity thickness. A slight shift in the absorbing wavelength for second and third order of cavity has been attributed to the slight change in the resonance frequency of the top metallic pattern due to the change in

separation between the top and bottom layers. The surface current distributions at the top and bottom metallic layers for the first three orders of cavity thickness are shown in Figs. 2.4(a)-(c) respectively.

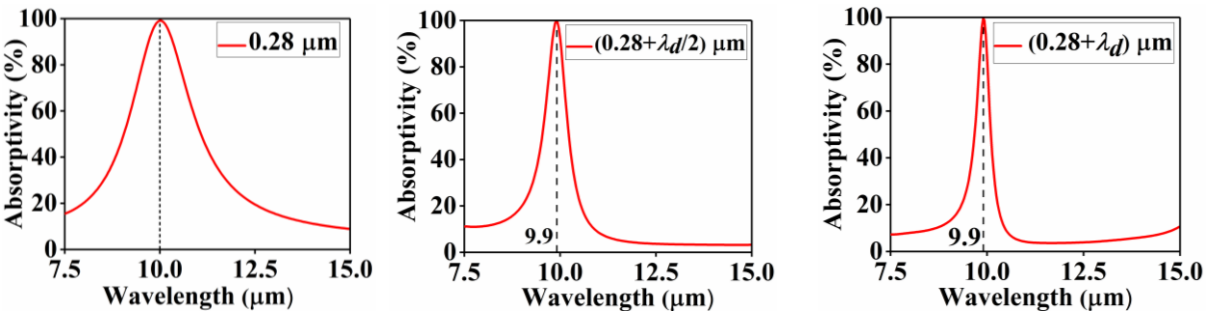

Fig. 2.3. Absorptivity response for the first three order of cavity thickness (a) t_{d1} = 0.28 μm (b) t_{d2} = 2.38 μm (c) t_{d3} = 4.48 μm.

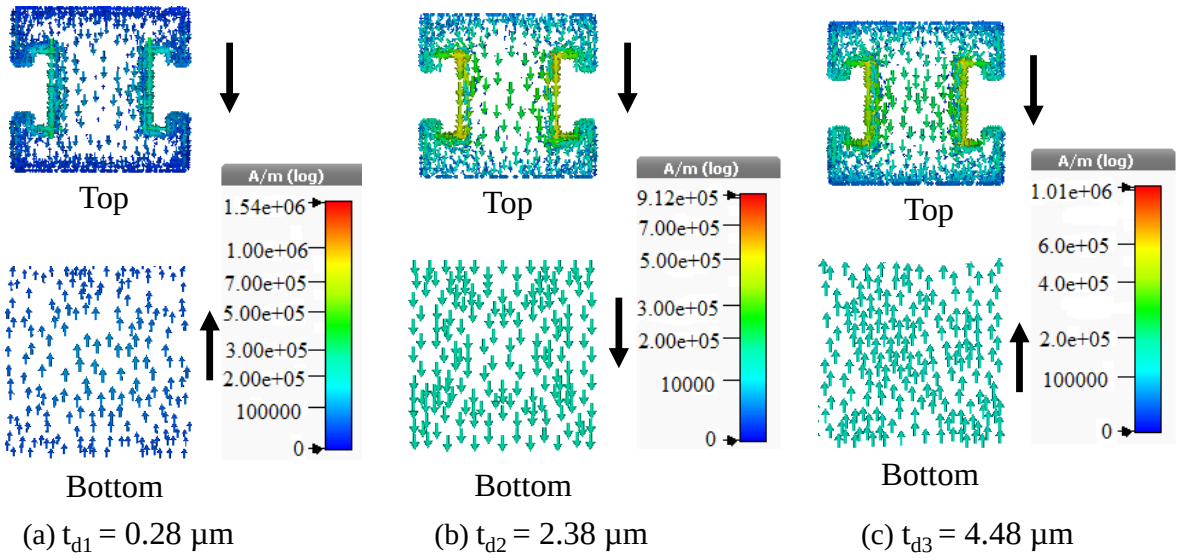

Fig. 2.4. Surface current distributions at the top resonating metasurface and bottom metallic reflector for the first three orders of cavity thickness (a) t_{d1} = 0.28 μm (b) t_{d2} =2.38 μm (c) t_{d3} =4.48 μm.

It can be seen that for t_{d1} = 0.28 μm and t_{d3} = 4.48 μm i.e., for the 1st and 3rd order of cavity thickness, there is perfect absorption, when the surface currents at the top and bottom metallic plates are antiparallel to each other; while, for t_{d2} = 2.38 μm i.e., for the 2nd order of cavity

thickness, there is perfect absorption when the surface currents at the top and bottom metallic plates are parallel to each other. This contradicts the single model theory of metamaterial absorber, which suggests that for perfect absorption occurrence of antiparallel surface current is mandatory.

2.4. Study of surface current orientations

In order to elucidate the reason for parallel and antiparallel surface currents, the Fabry-Perot resonance inside the cavity for the first three orders of cavity thickness has been studied. This is done by observing the real part of E_x component along the *z*-direction extending from $z = 0$ i.e., bottom metallic reflector to $z = (0.035 + t_{dn})$ µm i.e., the top metasurface.

The tangential electric field component E_x has been studied for t_{d1} = 0.28 µm, t_{d2} = 2.38 µm and t_{d3} = 4.48 µm by considering the boundary conditions at the top and bottom metallic surfaces. The electric field component corresponding to first three orders of cavity thickness are shown in Figs. 2.5(a)-(c) respectively.

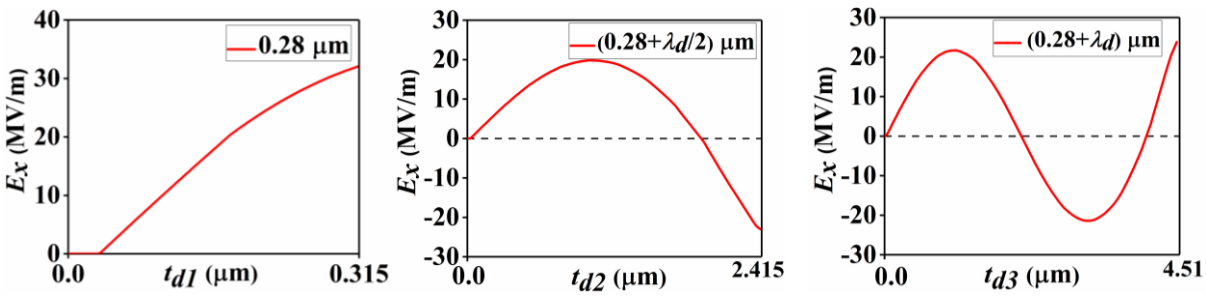

(a) (b) (c)

Fig. 2.5. Distribution of real part of E_x component along z direction for the first three order of cavity thickness (a) t_{d1} = 0.28 µm (b) t_{d2} =2.415 µm (c) t_{d3} =4.515 µm.

It can be observed from Fig. 2.5(a), that for the first order of cavity thickness E_x maintains a positive nonzero value at $z = 0.315$ µm, which decreases monotonically to zero at $z = 0$. The non-zero magnitude of E_x at $z = 0.315$ µm implies the quasi-open boundary due to the presence of patterned metallic structures on the top of the metasurface while the zero electric field at

$z = 0$ reveals closed boundary condition due to the bottom metallic reflector. The variation of the electric field component for the second order cavity is illustrated in Fig. 2.5(b), in which a half-sinusoidal cycle has been added to that of the first order cavity; thereby forming a second-order Fabry-Perot resonant mode. Similarly, a full sinusoidal cycle has been added to the E_x distribution curve of the first order cavity thickness, leading to a third order resonance mode as shown in Fig. 2.5(c). It has also been found from Fig. 2.5 that the E_x components are in phase at the two boundaries for first and third orders of cavity while in the second order of cavity, they are out of phase. The relations between surface currents and electric field at the top and bottom metallic plates are given by equations (2.6) and (2.7) respectively.

$$J_{x,metasurface} = j\omega\varepsilon_{metasurface}E_x \tag{2.6}$$

$$J_{x,reflector} = j\omega\varepsilon_{reflector}E_x \tag{2.7}$$

It is evident from the equations that the surface currents at the top and bottom metallic layers are decided by the phase of the tangential electric field component E_x at the two layers and the sign of the effective permittivity. The permittivity of the bottom metallic reflector, $\varepsilon_{refelctor}$ is negative according to the Drude model.

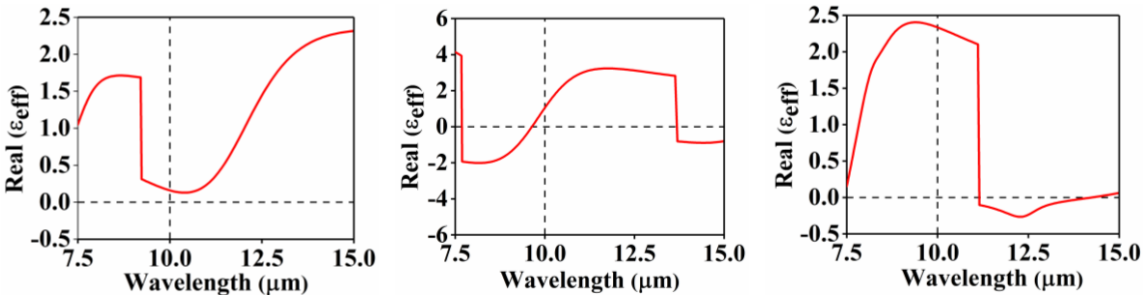

Fig. 2.6. Real part of effective permittivity of top resonating metasurface at the operating wavelength 10 μm for the cavity thickness (a) t_{d1} = 0.28 μm (b) t_{d2} =2.38 μm and (c) t_{d3} =4.48 μm.

The permittivity of the top metasurface is obtained by simulating the air/metasurface/dielectric configuration [61] The simulated reflection and transmission data is used to retrieve the permittivity of top metasurface [62]. The retrieved real part of permittivity values of metasurface layer for all three orders of cavity thickness are shown in Figs. 2.6(a)-(c).

It can be seen that the value of $\varepsilon_{metasurface}$ for all the three cases comes out to be positive at 10 μm. For the cavity thickness, t_{d1} = 0.28 μm and t_{d3} = 4.48 μm, E_x is in phase at the two boundaries of the cavity as shown in Fig. 2.5(a) and Fig. 2.5(c) respectively, whereas the value of permittivity of the top metasurface and bottom metallic reflector are opposite to each other. This gives rise to opposite signs of $J_{x,metasurface}$ and $J_{x,reflector}$ signifying anti-parallel surface currents at the two metallic plates. On the other hand, for $t_{d2} = 2.38\,\mu m$, the out-of-phase E_x values at the two boundaries of the cavity provide identical signs of $J_{x,metasurface}$ and $J_{x,reflector}$; thereby causing parallel surface currents at the top and bottom surfaces of the proposed structure.

2.5. Time-domain analysis of multiple reflections

To validate the multiple reflection phenomena existing inside the metamaterial absorber, a time domain analysis of metamaterial absorber under normal as well as oblique incidence conditions has been carried out. The simulated reflection coefficient (S_{11}) data of the metamaterial absorber is converted from frequency domain to time domain using the inverse chirp-Z transform technique [63]. For this purpose, a separate MATLAB code has been written, considering all the necessary conditions [64]. For the time domain analysis, the metamaterial absorber for third-order cavity thickness ($t_{d3} = 4.48\,\mu m$) has been considered. The schematic diagram showing multiple reflection phenomena in the metamaterial structure for normal incidence has been shown in Fig. 2.7(a). The distance between the top metasurface and incident port is considered as $h = 12$ μm to imply that the wave front is planar in nature.

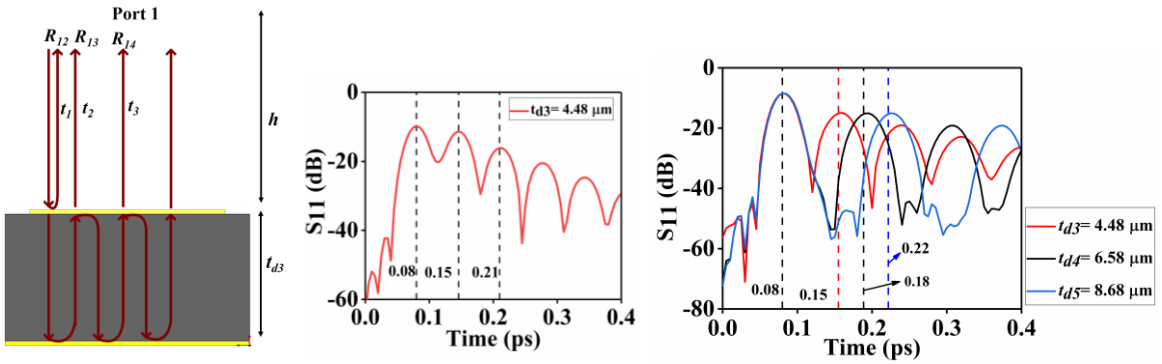

(a) (b) (c)

Fig. 2.7. (a) Multiple reflection phenomenon in the metamaterial absorber for normal incidence (b) time-domain analysis of the reflection coefficient of the metamaterial absorber for normal incidence (c) comparative study of Time-domain response of the reflection coefficient of 3rd, 4th and 5th order of cavity thickness.

A part of the wave reflected to port 1 (input port) at time t_1 after its first interaction with the metasurface is considered as R_{12}. The wave reflected to Port 1 at time t_2 and t_3 after striking bottom metallic reflector once and twice is shown as R_{13} and R_{14} respectively. The converted time domain response of the reflection coefficient (S_{11}) for the normal incidence case is shown in Fig. 2.7(b). The time of occurrence of each successive peak as shown in Fig. 2.7(b) corresponds to the time of occurrence of each of the reflected waves as shown in Fig. 2.7(a). The first peak obtained at 0.08 ps corresponds to the time of occurrence of the first reflected wave i.e., R_{12}. Similarly, the peaks obtained at 0.15 ps and 0.215 ps correspond to the times of occurrences of the second and the third reflected waves i.e., R_{13} and R_{14} respectively**.** The results obtained by time-domain analysis has also been analytically validated through equations (2.8-2.10). The time of occurrence of the first reflected wave R_{12} at port 1 can be computed from (2.8) where c is the velocity of the electromagnetic wave in free space. The times of occurrences of second R_{13} and third reflected waves R_{14} towards the port 1 can be

simultaneously computed employing equations (2.9) and (2.10) respectively, where ε_r is the relative permittivity of the dielectric.

$$t_1 = \frac{2h}{c} \tag{2.8}$$

$$t_2 = t_1 + \frac{2t_{d3}\sqrt{\varepsilon_r}}{c} \tag{2.9}$$

$$t_3 = t_2 + \frac{4t_{d3}\sqrt{\varepsilon_r}}{c} \tag{2.10}$$

For $h = 12$ µm and $t_{d3} = 4.48$ µm, the times of occurrences of first three reflected wave, mentioned as t_1, t_2 and t_3 in equations (2.8-2.10) have been analytically obtained as 0.08 ps, 0.1506 ps and 0.2212 ps respectively. These values are quite close to the ones obtained in the time-domain response as shown in Fig. 2.7(b). A comparative study of the time-domain responses for 3rd, 4th and 5th orders of Fabry-Perot cavity thicknesses have been studied and shown in Fig. 2.7(c). It has been found that the time of occurrence of first peak is same irrespective of the order of the cavity. This is quite obvious since R_{12} remains invariant to the cavity thickness as the distance between the top metasurface from the incident port remains unaltered. The times taken by the second and third peaks increase with increase in the cavity thickness.

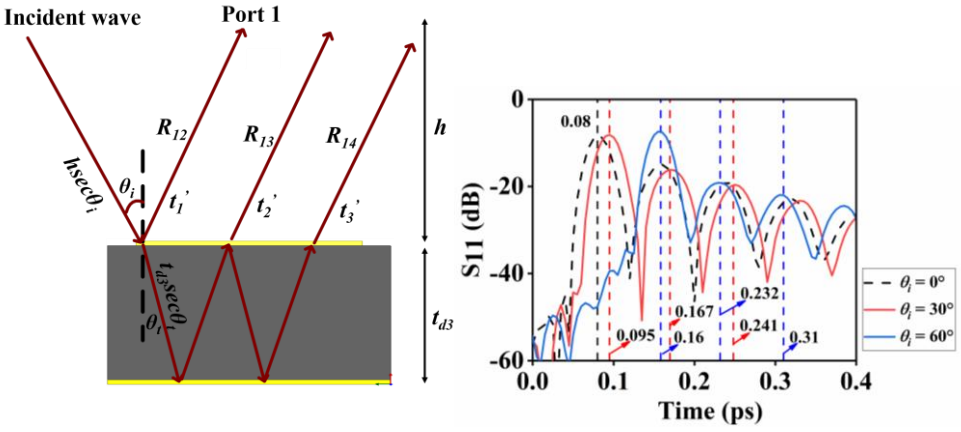

(a) (b)

Fig. 2. 8. Multiple reflection phenomenon in the metamaterial absorber for oblique incidences (b) time-domain analysis of the reflection coefficient peaks of metamaterial absorber for oblique incidences of 30º and 60º.

The time-domain response of the reflection coefficient has been further studied for oblique incidence case as shown in Fig. 2.8(a). During oblique incidence, the times of occurrences of peaks change due to change in the path length travelled by the electromagnetic wave. If the wave is incident at an angle θ_i on the top metasurface, the path travelled by the electromagnetic wave will be modified to $h\sec\theta_i$ instead of *h*. Similarly, the path travelled by the wave inside the cavity will be modified to $t_{d3}\sec\theta_t$ instead of t_{d3}. This leads to the increment of time of occurrences of the peaks under oblique incidence condition. The times of occurrences of first three peaks for the oblique incidence case can be computed as t_1', t_2' and t_3' using equations 2.11, 2.12 and 2.13 respectively.

$$t_1' = \frac{2h\sec\theta_i}{c} \tag{2.11}$$

$$t_2' = t_1' + \frac{2t_{d3}\sec\theta_t\sqrt{\varepsilon_r}}{c} \tag{2.12}$$

$$t_3' = t_2' + \frac{4t_{d3}\sec\theta_t\sqrt{\varepsilon_r}}{c} \tag{2.13}$$

The simulated reflection coefficient (S_{11}) data for the two oblique angular incidences of 30º and 60º in frequency domain have been converted into the time-domain ones. The time-domain response of the reflection coefficient has been illustrated in Fig. 2.8(b). For 30º angle of incidence, the time of occurrences of the first three peaks at port 1 is 0.092 ps, 0.162 ps and 0.234 ps respectively, whereas the times of occurrences of the first three peaks at port 1 for an angle of incidence of 60º are 0.16 ps, 0.235 ps and 0.31 ps respectively. The time domain data obtained numerically and presented in Fig. 2.8(b) have been verified with those obtained

analytically using equations (2.10-2.13). It has been found that the data obtained through both the methods are in close agreement.

2.5. Conclusions

Single-layer effective model based on antiparallel surface currents cannot provide a mathematical interpretation of absorption inside a metasurface absorber. For the better insight of absorption in such structures it is very much necessary to study the wave propagation in the form of electromagnetic fields. We have demonstrated metamaterial absorption based on three-layer effective model explaining the multiple reflection and interference phenomenon inside the dielectric layer. The constructive interference phenomenon between the multiple reflected waves inside the dielectric layer is responsible for the formation of Fabry-Perot resonance modes. The repetition of absorption characteristics of the structure with an increment of dielectric layer thickness by an integral multiple of a half-wavelength has been well explained in the light of formation of higher orders of resonating modes. The existence of higher order Fabry-Perot resonating modes confirms that the anti-parallel surface currents at the top and bottom layers are not the mandatory conditions for achieving the absorption phenomenon. To validate the multiple reflection phenomenon in the metamaterial absorber, time-domain analysis of reflection coefficient parameter using inverse chirp-Z transform technique has been implemented for both normal as well as oblique incidences. It has been found that the results obtained numerically through the time-domain conversion of refection coefficients are in good agreement with the analytical results.

CONTENTS

Chapter 3: Mathematical interpretation of wave propagation, standing wave resonance and absorption in a metasurface absorber